Laser and Particle Beams (2010), *28*, 575–583.

doi:10.1017/S0263034610000649

Production of high-intensity proton fluxes by a 2ω Nd:glass laser beam

J. BADZIAK,[1] S. JABŁOŃSKI,[1] P. PARYS,[1] A. SZYDŁOWSKI,[2] J. FUCHS,[3] AND A. MANCIC[3]

[1]Institute of Plasma Physics and Laser Microfusion, EURATOM Association, Warsaw, Poland
[2]The Andrzej Soltan Institute for Nuclear Studies, Świerk, Poland
[3]LULI, Ecole Polytechnique, CNRS, CEA, UPMC, Palaiseau, France

(Received 6 August 2010; Accepted 16 October 2010)

Abstract

The results of numerical and experimental studies of high-intensity proton beam generation using a 2ω or 1ω Nd:glass laser beam irradiating a thin hydrogen-rich target are reported. The effect of the laser wavelength (λ), intensity (I_L) and pulse duration as well as the target thickness, and the preplasma density gradient scale length on proton beam parameters, and the laser-protons energy conversion efficiency were examined by particle-in-cell simulations. Both the simulations and measurements, performed on the LULI 100 TW laser facility at I_L up to 2×10^{19}W/cm^2, prove that at the $I_L\lambda^2$ product fixed, the 2ω laser driver can produce proton beams of intensity, current density and energy fluence significantly higher than the ones which could be achieved using the 1ω driver. In particular, at $I_L\lambda^2\sim(0.5–1)\times10^{20}$ Wcm^{-2} μm^2 the 2ω picosecond driver makes it possible to generate multi-MeV proton beams of intensity and current density in excess of 10^{21}W/cm^2 and 10^{14}A/cm^2, respectively, with the conversion efficiency above 10%.

Keywords: Laser-driven ion acceleration; Laser-produced plasma; Ponderomotive force; Proton beams; Radiation pressure

1. INTRODUCTION

The application of laser-accelerated ions in high energy-density physics and for fast ignition (FI) of fusion targets require collimated ion beams of relatively low ion energies (≤10 MeV) but of very high power P_i and intensity I_i (for instance, FI requires MeV proton beams of $I_i\sim10^{20}$ W/cm^2 and $P_i\sim1$ PW (Temporal *et al.*, 2002; Badziak *et al.*, 2007)). Potentially, the ion beams of such extreme parameters can be produced by currently known laser methods of ion acceleration such as target normal sheath acceleration (TNSA) (Wilks *et al.*, 2001; Borghesi *et al.*, 2006; Badziak 2007; Yang *et al.*, 2010) or skin-layer ponderomotive acceleration (SLPA) (Badziak *et al.*, 2004, 2005, 2006, 2008; Badziak 2007; Hora *et al.*, 2002; Sadighi-Bonabi *et al.*, 2010) (also referred to as radiation pressure acceleration (RPA) (Liseykina & Macchi, 2007; Robinson *et al.*, 2008; Liseykina *et al.*, 2008). In TNSA, ions are accelerated at the rear surface of the foil target by a virtual cathode (Debye sheath) created by hot electrons produced by a laser pulse at the target front and penetrating through the target. Though at relativistic laser intensities I_L (i.e., at $I_L\lambda^2 > 10^{18}$ Wcm^{-2}μm^2, where λ is the laser wavelength) TNSA can produce collimated ion beams of fairly high ion energies (of tens of MeV for protons (Borghesi *et al.*, 2006; Badziak, 2007; Snavely *et al.*, 2000; Robson *et al.*, 2007)) or of several MeV/amu for heavier ions (Badziak, 2007; Hegelich *et al.*, 2005; McKenna *et al.*, 2007), the ion density of TNSA beams is relatively low (≤10^{19}cm^{-3} at the source) and, as a result, the ion beam intensity $I_i = n_i v_i E_i$ or current density $j_i = zen_iv_i$ are usually moderate (z is ion charge state, e is the elementary charge, n_i, v_i, E_i are ion density, velocity and energy, respectively). In turn, SLPA employs the ponderomotive pressure induced by a laser pulse near the critical plasmas surface, which drives forward a dense plasma (ion) bunch of density n_i higher than the plasma critical density n_c. As for relativistic laser intensities usually $n_i \geq 10^{22}$ cm^{-3}, the intensities and current densities of SLPA-driven ion beams can be much higher than in the case of TNSA beams, in spite of the fact that SLPA-driven ions are usually a few times slower than those generated by TNSA (Badziak *et al.*, 2004, 2005, 2008; Badziak, 2007). Moreover, SLPA-driven ions can be extracted from a fairly

Address correspondence and reprint requests to: J. Badziak, Institute of Plasma Physics and Laser Microfusion, EURATOM Association, 23 Hery Street, 01-497 Warsaw, Poland. E-mail: badziak@ifpilm.waw.pl

thick solid-density layer (of the thickness of several μm or even thicker at multi-ps driving pulses), thus a large number of ions can be generated from the source of a small area (S_s), much smaller than in the case of TNSA (or the methods using ultrathin targets like e.g., the laser break-out after burner (Yin *et al.*, 2006; Fernandez *et al.*, 2009), where the ions are efficiently extracted from the layer of only several to tens nm (Roth *et al.*, 2002; Allen *et al.*, 2004; Foord *et al.*, 2007). The last feature of SLPA is especially important for application of ion beams for FI research, where a huge number of high-energy ions are required to ignite a Deuterium-Tritium fuel. For instance, $(2–3)\times10^{16}$ protons of mean energy $\bar{E}p \approx 3–5$ MeV necessary for the fuel ignition (Temporal *et al.*, 2002; Badziak *et al.*, 2007) can be produced by SLPA from a hydrogen-rich target of $S_s \leq 0.05$ mm^2, while it needs S_s at about a few mm^2 when using TNSA (Badziak *et al.*, 2007). As a result, the laser power P_L required for the ignition ($P_L \propto I_L S_s$) and the proton source-fuel distance $d_{sf} \sim S_s^{1/2}$ can be significantly smaller when using SLPA-driven ion beams (the last feature benefits, in particular, in the permissibility of using non-monoenergetic proton beams for the ignition (Badziak *et al.*, 2007)). One of the questions is the laser-SLPA protons energy conversion efficiency that is still open.

At relativistic laser intensities and experimental conditions currently attainable, both TNSA and SLPA can contribute to the forward ion acceleration, and they particular contribution to this process depends on laser and target parameters. In the case of proton acceleration by an infrared (~1μm), linearly polarized laser pulse usually TNSA dominates (Allen *et al.*, 2004; Robson *et al.*, 2007; Fuchs *et al.*, 2007), and SLPA can be efficient only when some specific requirements are met (Badziak *et al.*, 2004; Badziak, 2007; Sentoku *et al.*, 2002; Lee *et al.*, 2008) : (1) the target is made of hydrogen-rich insulator (to minimize the return electron current enabling effective transport of hot electrons through the target); (2) the preplasma density gradient scale length near the critical surface, L_n, is small, say $L_n \leq 2\lambda$, but still $L_n >> l_s$, where l_s is the skin depth (to ensure small Debye length near the critical surface and high value of the ponderomotive force); (3) the laser beam direction is perpendicular to the target front surface and the beam diameter on the target, d_L, is sufficiently large: $d_L >> L_n, \lambda_L, L_T$, where L_T is the target thickness (to ensure quasi-planar acceleration geometry enabling generation of low-divergence ion beam). The particular contribution of SLPA and TNSA to the acceleration process also depends on laser light polarization and for circular polarization the role of TNSA is less important than for the linear one (Liseykina & Macchi, 2007; Liseykina *et al.*, 2008).

In a great majority of laser acceleration experiments or numerical simulations performed so far, fundamental-frequency (1ω) beams of Nd:glass or Ti:sapphire lasers have been used as an ion driver. This is due to the fact that the dimensionless laser field amplitude $a_0 \propto I_L^{1/2}\lambda$, which is the most important factor determining maximum energy of accelerated ions, is higher for a 1ω laser beam than for short-wavelength (2ω or 3ω) beams. On the other hand, using 2ω or 3ω beams enables to achieve a higher laser pulse contrast ratio and, as a result, a sufficiently small value of L_n, which, in particular, is desirable for an efficient SLPA. Moreover, the critical density is higher for the short-wavelength beams (it scales as $(1+a_0^2/2)^{1/2}\ \lambda^{-2}$ (Umstadter, 2001)), which suggests that attainable ion current densities and beam intensities of SLPA-driven ions can be higher as well (at least when the values of a_0 are not very different for 1ω and 2ω (3ω) beams). These possible advantages of short-wavelength lasers as ion drives seem to be especially important for FI-related ion beam applications, where maximizing the ion beam intensity (current density) at moderate ion energies is desirable and high laser contrast is necessary to avoid the ion target destruction by the prepulse of a multi-kJ short-pulse laser. However, the above issues have not riveted enough attention and have not been investigated in detail so far.

In this paper, we compare parameters of proton beams produced at the interaction of either 1ω or 2ω laser beam of relativistic intensity with a thin hydrogen-rich target. The results of measurements as well as numerical, hydrodynamic, and particle-in-cell (PIC) simulations are presented. In particular, it is shown that the contribution of the SLPA mechanism to the ion acceleration process is higher for the 2ω driver than for the 1ω one, which results in significantly higher intensity and current density of the accelerated protons.

2. RESULTS OF PIC SIMULATIONS

For the simulations, a fully electromagnetic, relativistic one-dimensional (1D) PIC code very similar to the well known LPIC ++ code (Holkundkar & Gupta, 2008) was used. A linearly polarized laser pulse of quasi-Gaussion pulse shape ($I_L \propto \exp[-t^4]$) interacted with an inhomogeneous, fully ionized hydrogen plasma layer of the density profile defined by the exponential front part (the preplasma layer) of the density gradient scale length L_n and the constant part of the density $n_e = n_i = 4\times10^{22}$ cm^{-3} and the thickness L_T. The simulations were performed for laser pulses of the wavelengths corresponding to the first (1ω) and second (2ω) harmonic of Nd:glass laser, of duration from 0.35 ps to 2 ps and intensities up to about 5×10^{20} W/cm^2 . Depending on the initial parameters the space z of the simulations was ranged from 22.8 μm to 50.6 μm, the number of Euler cells from 8570 to 19220 and the number of macro particles from 53259 to 828138.

Figures 1 and 2 present peak values of various parameters of proton beams, generated from a 1-μm hydrogen plasma target of $L_n = 1$ μm or 0.25 μm, by 0.35-ps (full width at half maximum) laser pulses of different wavelengths, as a function of the $I_L\lambda^2$ product (this product is proportional to the square of the dimensionless laser field amplitude $a_0^2 \approx 0.73\times10^{-18} I_L\lambda^2$[Wcm^{-2},μm] and is usually used for

https://doi.org/10.1017/S0263034610000649 Published online by Cambridge University Press

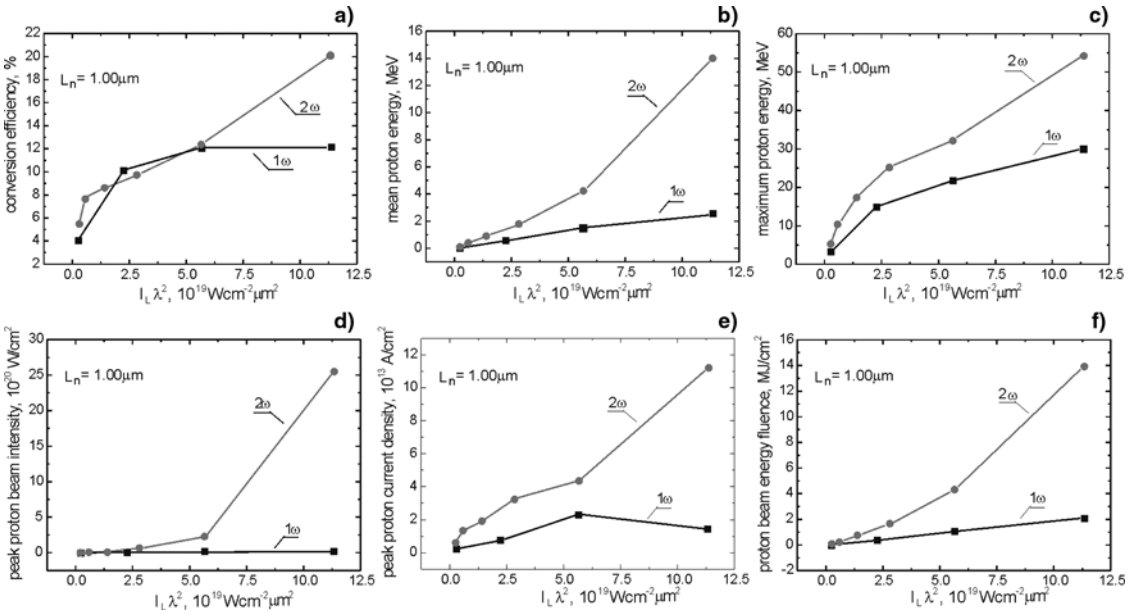

Fig. 1. Parameters of proton beams driven by 1ω or 2ω Nd:glass laser pulses as a function of $I_L\lambda^2$. $L_T = 1\mu m$, $L_n = 1\mu m$, $\tau_L = 0.35ps$.

scaling). Excluding the laser-protons energy conversion efficiency η at low laser intensities, where η for 1ω and 2ω are comparable, the parameters of a proton beam driven by the 2ω laser beam are significantly higher than those for the 1ω beam, and the highest values of these parameters are attained for the short density gradient scale length. In particular, for $I_L\lambda^2 \geq 5 \times 10^{19}$ $Wcm^{-2}\mu m^2$, the peak proton beam intensity and peak current density for protons driven by 2ω reach the values in excess 10^{21} W/cm^2 and 10^{14} A/cm^2, respectively. One of the reasons for such extreme values of these parameters is the high value of the plasma critical density at 2ω enabling ponderomotive acceleration of a very dense proton (plasma) bunch.

The effect of the target thickness, L_T, on the parameters of proton beams driven by laser pulses of different durations and wavelengths but fixed value of the dimensionless laser amplitude ($I_L\lambda^2 = 5 \times 10^{19}$ $Wcm^{-2}\mu m^2$) is shown in Figure 3. For the optimum target thicknesses, the conversion efficiencies are similar for 1ω and 2ω, but the remaining parameters are considerably higher for the shorter wavelengths. Moreover, for the 1ω beam high values of the proton beam parameters are observed only for very thin (<1 μm) targets

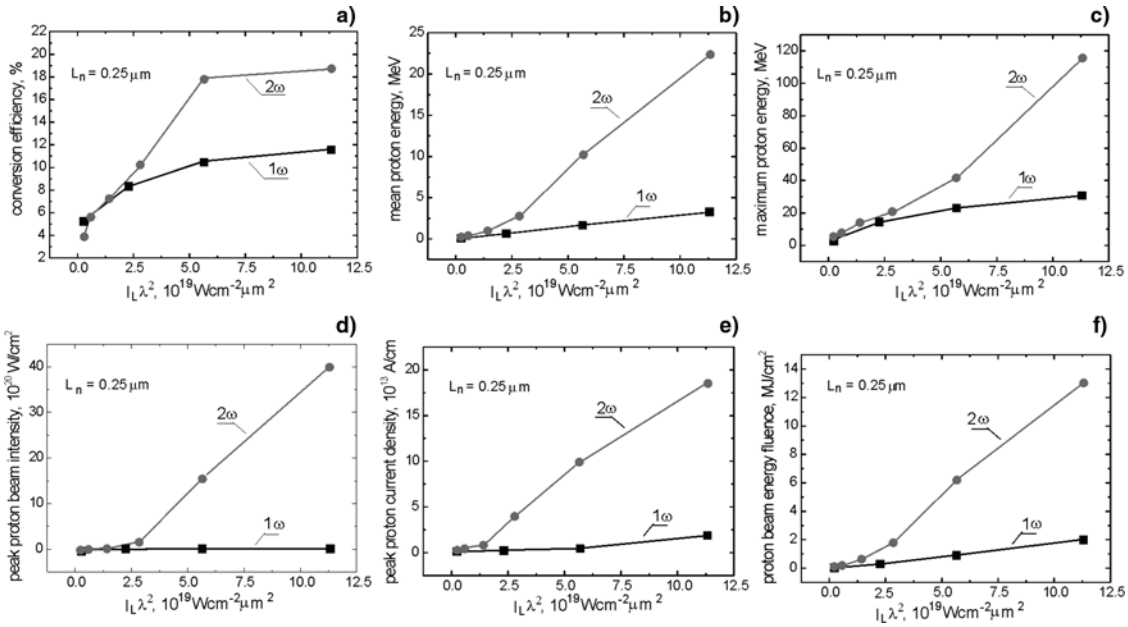

Fig. 2. As for Figure 1 but $L_n = 0.25$ μm.

https://doi.org/10.1017/S0263034610000649 Published online by Cambridge University Press

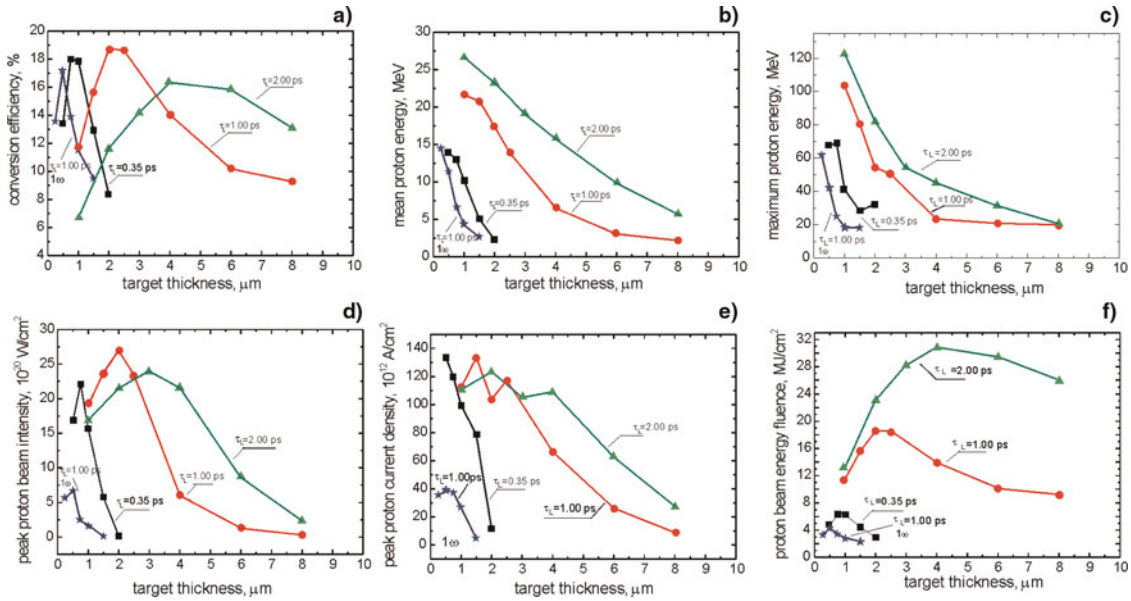

Fig. 3. (Color online) Parameters of proton beams driven by laser pulses of different durations and wavelengths as a function of the target thickness. $I_L\lambda^2 = 5\times10^{19}\mathrm{Wcm}^{-2}\mu\mathrm{m}^2$, $L_n = 0.25$ μm.

and for a narrow range of L_T, while shortening of the wavelength results in a shifting the optimum L_T toward much thicker targets and in a broadening the L_T range with high proton beam parameters and high conversion efficiency. The optimum target thickness grows with the laser pulse duration (in general, with the laser energy fluence $F_L \approx I_L\tau_L$). In particular, it suggests that using 2ω multi-ps laser pulses of $I_L\lambda^2 \sim (0.5\text{–}1)\times10^{20}$ $\mathrm{Wcm}^{-2}\mu\mathrm{m}^2$ makes it possible to produce ultraintense proton beams with high conversion efficiency from the targets of the thickness of a few tens of

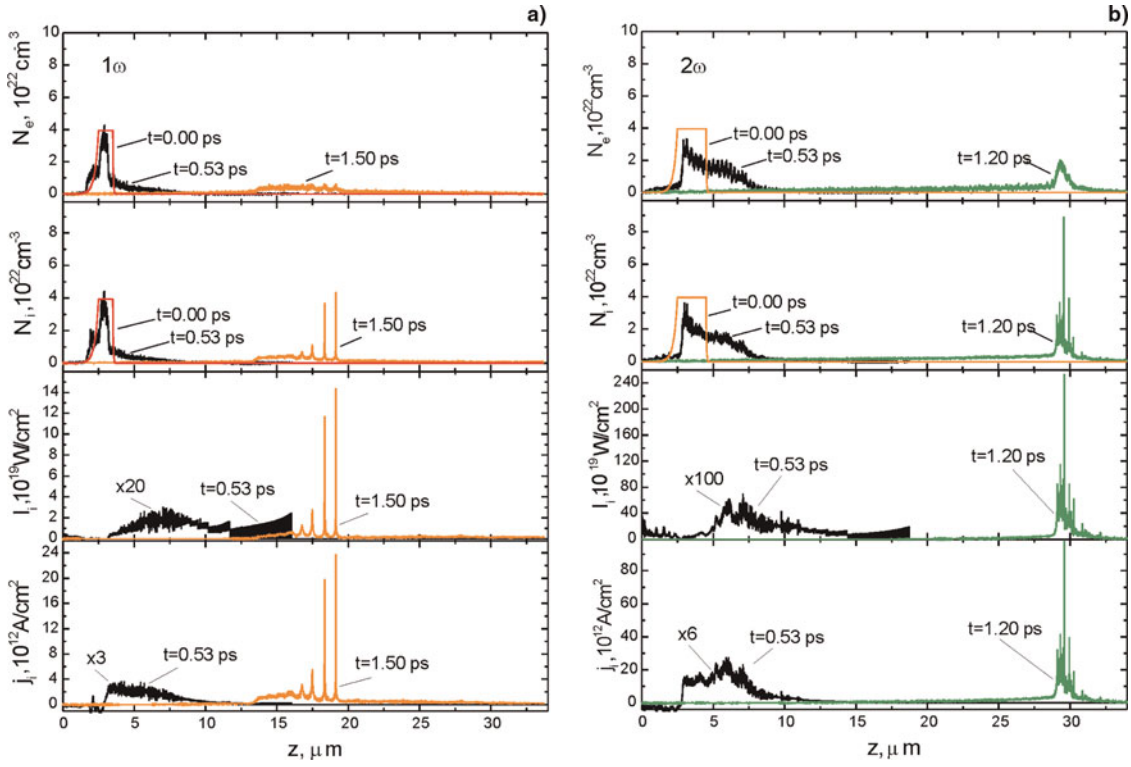

Fig. 4. (Color online) Spatial distributions of the electron (N_e) and proton (N_i) density as well as the proton beam intensity (I_i) and current density (j_i) at different instants t for the case of 1ω (**a**) and 2ω (**b**) driver. $I_L\lambda^2 = 5\times10^{19}\,\mathrm{Wcm}^{-2}\mu\mathrm{m}^2$, $\tau_L = 1$ps, $L_n = 0.25$ μm.

https://doi.org/10.1017/S0263034610000649 Published online by Cambridge University Press

μm. It is an important practical advantage of a 2ω driver from the point of view of a possible application of the accelerated proton beam in FI-related and other high-energy laser experiments, which require robust targets, resistant to damage by the laser prepulse or other (e.g., X-ray) radiations.

The very high intensities and current densities of proton beams driven by the 2ω beam result particularly from the fact that in the case of a short-wavelength driver, even at a moderate value of the dimensionless laser amplitude $a_0 \sim 5–10$, SLPA can dominate over TNSA and, as a consequence, the proton beam can be more dense and compact in space. It is due to the fact that the temperature of laser-produced hot electrons, T_h, which is the factor determining efficiency of the TNSA mechanism, increases with an increase in λ (Wilks *et al.*, 2001; Borghesi *et al.*, 2006) while the radiation (ponderomotive) pressure is λ-independent and proportional to I_L (Denevit, 1992; Badziak *et al.*, 2008). Thus, the shortening of laser wavelength at $I_L\lambda^2 = \text{const.}$ leads to quite rapid diminishing of the TNSA efficiency while the SLPA efficiency remains fixed. As a result, when λ is sufficiently small the contribution of TNSA to the ion acceleration process can be smaller than that of SLPA.

A formation of high-intensity proton bunches driven by the 1ω and 2ω laser beams of $I_L\lambda^2 = 5 \times 10^{19}\text{Wcm}^{-2}\mu\text{m}^2$ is illustrated in Figure 4. The figure presents spatial (along the propagation direction z) distributions of the electron density (N_e), the ion density (N_i), the beam intensity (I_i), and the ion current density (j_i) for two different instants (t) of the acceleration process ($t = 0$ corresponds to the beginning of the laser-target interaction). In the case of the 1ω driver, where the TNSA contribution to the acceleration process is significant, most of ions (and electrons) are spread in space in the late phase of acceleration and only a small part of the ions driven (indirectly) by the ponderomotive pressure forms relatively dense and intense ion spikes. In the case of the 2ω driver, a remarkable part of the target plasma is strongly compressed by the ponderomotive pressure and accelerated in the form of well localized in space, very dense and very intense plasma bunch. Although there is still a subtle, multi-shock structure visible in the bunch and part of the accelerated ions is situated outside the bunch, its intensity and current density are much higher than for the case of the long-wavelength (1ω) driver. The proton pulse duration is very small and at the distance ~20–30 μm from the target the duration is below 100 fs. Though such a short pulse is also produced in the 1ω case, however the amount of protons in the compressed bunch is much smaller here than in the 2ω case.

3. RESULTS OF EXPERIMENT AND A COMPARISON WITH NUMERICAL SIMULATIONS

In the experiment, performed on the LULI 100 TW Nd:glass laser facility at Ecole Polytechnique (Palaiseau, France) a 1ω or 2ω Nd:glass laser pulse of high contrast ratio (~10^7 for 1ω and > 10^8 for 2ω), of 350-fs duration and intensity up to 2×10^{19} W/cm^2 irradiated a thin (0.6–1 μm) polystyrene (PS) target along the target normal. Since the preplasma density gradient scale length near the critical surface, L_n, was relatively small ($L_n < 3$ μm for 1ω (Fuchs *et al.*, 2007) and $L_n < 1$ μm for 2ω) and the laser beam diameter on the target, d_L, was ≈ 15–50 μm (80% energy) and, moreover the target was made of insulator, the conditions required for efficient SLPA were quite well fulfilled, especially for larger d_L and/or 2ω laser beam. The proton beam characteristics were measured using the time-of-flight method (ion charge collectors (Badziak *et al.*, 2001)), solid state track detectors (SSTDs) and radiochromic films (RCFs). The characteristics of protons of low ($E_p < 0.1$ MeV) and moderate (0.1 MeV ≤ $E_p < 3$ MeV) energy were measured by four ion collectors (ICs) situated 80 cm from the target at the angles 1°, 4°, 8°, and 30° in respect to the target normal. High-energy protons (≥3 MeV) were recorded by SSTDs (CR 39 of PM 355 type (Szydłowski *et al.*, 2009) with Al filters) and the stack of RCFs of H-810 type (both these detectors were strongly saturated by moderate-energy protons at the target-detector distances employed: $L_{\text{SSTD}} = 123$ cm, $L_{\text{RCF}} = 2.5$ cm).

Figure 5 presents angular characteristics of a proton beam generated by the 1ω or 2ω laser beam for moderate-energy protons of 0.5 MeV < E_p < 3 MeV (a) and high-energy protons of $E_p \approx 3$ MeV (b, c) as measured by ICs (1) and RCFs (2, 3). In the case of moderate-energy protons driven by the 1ω beam, we observed a ring-like spatial structure of the proton beam for both lower (2×10^{18} W/cm^2) and higher (2×10^{19} W/cm^2) laser intensities as opposed to those driven by the 2ω beam for which the proton beam structure without any remarkable dip in the beam centre was recorded (Fig. 5a). In the case of high-energy protons, the situation was different. For the 2ω driving beam, the proton beam structure was rather flat independent on laser intensity

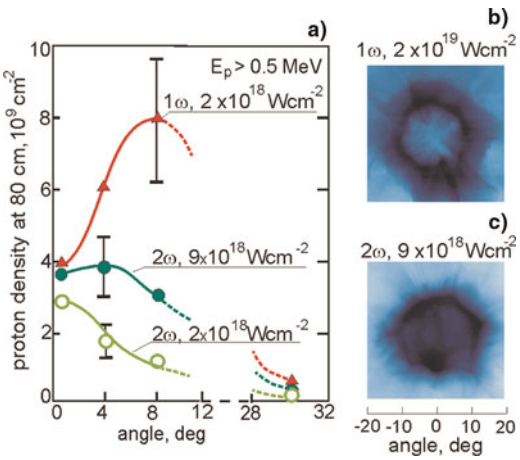

Fig. 5. (Color online) Angular characteristics of a proton beam generated by the 1ω or 2ω laser beam for (**a**) moderate-energy protons of 0.5 MeV < E_p < 3 MeV and (**b**, **c**) high-energy protons of $E_p \approx 3$ MeV.

https://doi.org/10.1017/S0263034610000649 Published online by Cambridge University Press

(Fig. 5c). However, for the 1ω beam, the flat spatial structure for high-energy protons was observed only at lower laser intensities, while at higher intensities the structure had always annular shape (Fig. 5b). The observed differences in the moderate-energy and high-energy proton beams structures can be explained assuming that moderate-energy proton acceleration is dominated by SLPA and high-energy protons are driven mainly by TNSA (Pukhov, 2001; Badziak *et al.*, 2008). This issue was discussed in detail in Badziak *et al.* (2008), so we only notice here that the ring-like structure of high-energy protons is likely due to the target rear surface perturbation by the prepulse-driven shock wave (Xu *et al.*, 2006), while the structure of moderate-energy protons is determined by the action of the ponderomotive force (F_p) near the critical surface (Wilks *et al.*, 1992; Badziak *et al.*, 2006).

The effect of the ponderomotive force on the structure essentially depends on the preplasma density gradient scale length L_n (Badziak *et al.*, 2006). For a small L_n (the 2ω case) and $d_L \gg L_n$, the radial component of F_p is small and, as a result, the proton beam of a low angular divergence and bell-shaped (Gaussion-like) spatial structure is generated (Badziak *et al.*, 2006). When L_n is larger (the 1ω case), the radial component of F_p is higher and the beam of a larger angular divergence and a ring-like structure can be produced (Badziak *et al.*, 2006). This feature of SLPA-driven proton generation is demonstrated in Figure 6, which presents the results of simulations, carried out with the use of two-dimensional (2D) relativistic hydro code (Badziak *et al.*, 2006), for protons driven by the 1ω or 2ω laser beam of parameters corresponding to those in the experiment. A fairly good qualitative agreement with the experimental results shown in Figure 5a can be seen.

A comparison of the proton beam intensities I_{ps} and current densities j_{ps} at the source and the laser-protons energy conversion efficiencies for moderate-energy (0.5–3 MeV or 1–3 MeV) protons driven by the 1ω or 2ω laser beam is presented in Figure 7. The values of I_{ps} and j_{ps} were calculated from the IC measurements using the formula (Badziak *et al.*, 2004, 2008): $I_{ps} \approx E_t/\tau_s S_s$, $j_{ps} \approx Q_t/\tau_s S_s$ where E_t and Q_t are the total energy and the total charge of protons in the considered energy range, respectively, τ_s is the proton pulse duration at the source and S_s is the proton beam area at the source. Since for SLPA ions τ_s is approximately equal to the laser pulse duration τ_L and S_s is close to the laser focal spot area $S_L = \pi d_L^2$ (Badziak *et al.*, 2004, 2005, 2006; Liseykina & Macchi, 2007; Habara *et al.*, 2003), to calculate I_{ps} and j_{ps} we assumed $\tau_s \approx \tau_L$, $S_s \approx S_L$. It can be seen that in the case when $I_L\lambda^2$ for the 1ω beam is equal to that for the 2ω beam, the beam intensity and current density of

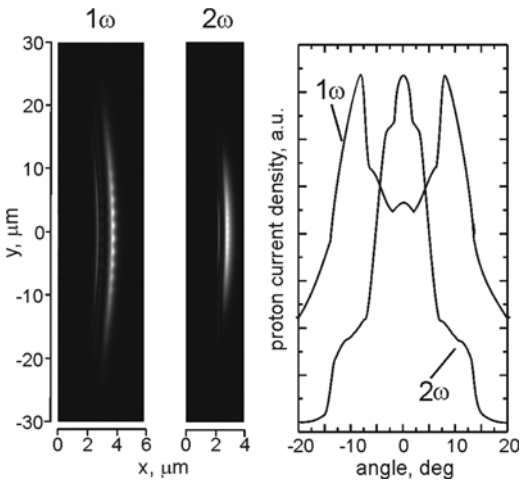

Fig. 6. The spatial and angular distributions of proton current densities for protons driven by the 1ω or 2ω laser beam — the results of simulations using 2D relativistic hydro code. $I_L^{1\omega} = I_L^{2\omega} = 2 \times 10^{18}$ W/cm^2, $d_L^{1\omega} =$ 30 μm, $L_n^{1\omega} = 1$ μm, $d_L^{2\omega} = 20$ μm, $L_n^{2\omega} = 0.25$ μm.

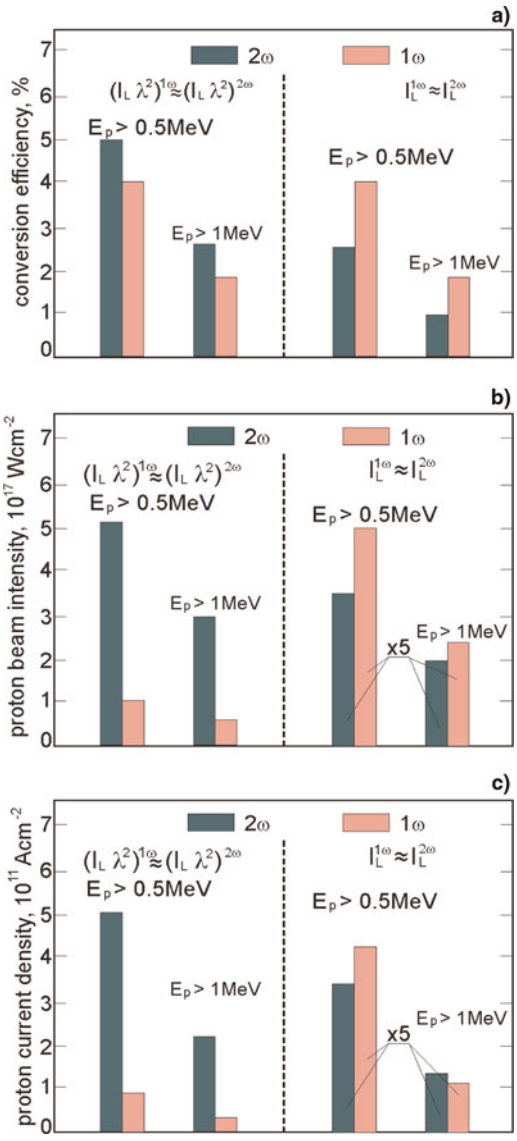

Fig. 7. (Color online) A comparison of laser-proton conversion efficiencies (**a**) as well as proton beam intensities (**b**) and current densities (**c**) at the source for moderate-energy (<3 MeV) protons generated by the 1ω or 2ω Nd:glass laser beam. The results obtained from the experiment at $I_L\lambda^2 \approx 2.1 \times 10^{18}$Wcm^{-2}μm^2, $\tau_L = 0.35$ ps, $L_T = 1$ μm.

https://doi.org/10.1017/S0263034610000649 Published online by Cambridge University Press

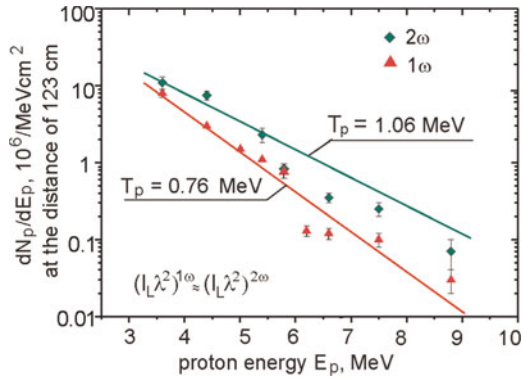

Fig. 8. (Color online) The energy distributions for high-energy protons driven by the 1ω or 2ω laser beam. Points — the results of SSTD measurements, lines — the results of approximation by the Maxwellian energy distributions with the temperature T_p. $I_L\lambda^2 \approx 2.1 \times 10^{18}$Wcm^{-2}μm^2, $\tau_L = 0.35$ ps, $L_T = 1$ μm.

moderate-energy protons are several times higher and the conversion efficiency is about 20–30% higher for the 2ω beam than those for the 1ω beam, in spite of the fact that the 2ω laser beam energy was more than twice as low. Also, the number (per cm^2) of high-energy (>3 MeV) protons is higher for 2ω in this case (Fig. 8). However, for $I_L^{1\omega} \approx I_L^{2\omega}$, the beam intensities and current densities of the moderate-energy protons are comparable for 1ω and 2ω and the laser-protons conversion efficiency is lower for the 2ω beam. These results are in fairly good agreement with our PIC simulations, which for the case $(I_L\lambda^2)^{1\omega} = (I_L\lambda^2)^{2\omega}$ and $E_p > 0.5$ MeV are presented in Figure 9. The values of the (average) beam intensity and current density where calculated here in the same way as for the experiment i.e., using the formulas: $I_{ps} \approx E_t/\tau_L S_L$, $j_{ps} \approx Q_t/\tau_L S_L$. It can be seen that for the anticipated most probable ranges of L_n: 1–3 μm for 1ω and 0.25–1 μm for 2ω, the beam intensities and current densities for the 2ω case are several (~4–6) times higher than the ones for the 1ω case, while the conversion efficiencies are comparable for both cases. Also the absolute values of the considered parameters are in a reasonable agreement with those estimated from the measurements. The observed accordance in the results of measurements and simulations is another argument which supports our earlier conclusion (Badziak *et al.*, 2008) that, in the conditions of our experiment, most of moderate-energy protons are driven by the SLPA mechanism. This conclusion is also proved by more detailed analysis of our PIC results which clearly show that relatively small number of protons is accelerated to high (multi-MeV) energies by TNSA while a bulk of protons (of lower energies) is driven by the ponderomotive pressure and the amount of these protons is higher for the 2ω driver.

4. CONCLUSIONS

In conclusion, both numerical simulations and measurements prove that the 2ω Nd:glass laser driver produces proton

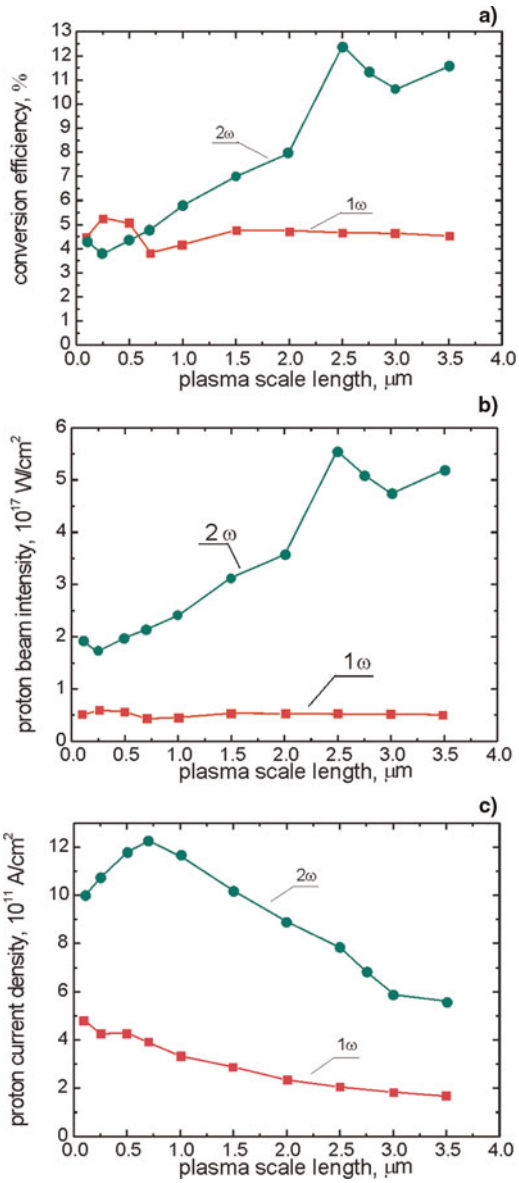

Fig. 9. (Color online) The laser-protons energy conversion efficiency as well as the proton beam intensity and current density at the source for the 1ω or 2ω laser driver as a function of the preplasma density gradient scale length L_n. The results of PIC simulations obtained at $I_L\lambda^2 = 2.1 \times 10^{18}$Wcm^{-2}μm^2, τ_L =0.35 ps, $L_T = 1$ μm.

beams of significantly higher intensity, current density, and energy fluence than those achieved with the use of the 1ω driver of the same value of the $I_L\lambda^2$ product. Even at moderate values of $I_L\lambda^2 \sim (0.5–1) \times 10^{20}$ Wcm^{-2}μm^2, the 2ω picosecond driver makes it possible to produce ultraintense, multi-MeV proton beams of intensity and current density in excess of 10^{21} W/cm^2 and 10^{14}A/cm^2, respectively. In this case, SLPA (RPA) clearly prevails other acceleration mechanisms and highly efficient ($\eta > 10\%$) generation of the ultraintense proton beams is possible from the targets several times thicker than for the 1ω case, which benefits in a higher areal proton density of the proton source and its greater robustness. In addition, a higher contrast ratio of the 2ω laser beam

https://doi.org/10.1017/S0263034610000649 Published online by Cambridge University Press

allows for generation of proton beams of more homogeneous spatial structure and for avoiding the target destruction by the laser prepulse. The above advantages of the 2ω driver indicate that it can be a promising laser driver of proton beams required for ICF fast ignition as well as high-current proton beams desirable for application in high energy-density physics or for isotope production. However, its significant advantages should always be considered in the context of its higher cost and, typically, up to ~30–40% lower laser energy than in the case of the 1Ω driver.

ACKNOWLEDGEMENTS

The authors acknowledge the LULI laser team as well as P. Antici and M. Rosiński for their expert support to the experiment. We also thank J. Wołowski for useful discussions. The access to the LULI 100TW laser facility has been supported by the European Commission under the LASERLAB-Europe Integrated Infrastructure Initiative (contract No. RII3-CT-2003-506350). This work was also supported in part by the HiPER project under Grant Agreement No. 211737 as well as by the Ministry of Science and Higher Education, Poland, under Grant No. N202-207-438.

REFERENCES

Allen, M., Patel, P.K., Mackinnon, A., Price, D., Wilks, S. & Morse, E. (2004). Direct experimental evidence of back-surface ion acceleration from laser-irradiated gold foils. *Phys. Rev. Lett.* **93**, 265004/1–4.

Badziak, J., Makowski, J., Parys, P., Ryć, L., Wołowski, J., Woryna, E. & Vankov, A.B. (2001). Intensity-dependent characteristics of a picosecond laser-produced Cu plasma. *J. Phys. D: Appl. Phys.* **34**, 1885–1891.

Badziak, J., Głowacz, S., Jabłoński, S., Parys, P., Wołowski, J. & Hora, H. (2004). Production of ultrahigh ion current densities at skin-layer subrelativistic laser-plasma interaction. *Plasma Phys. Contr. Fusion* **46**, B541–B555.

Badziak, J., Głowacz, S., Jabłoński, S., Parys, P., Wołowski, J. & Hora, H. (2005). Generation of picosecond high-density ion fluxes by skin-layer laser-plasma interaction. *Laser Part. Beams* **23**, 143–147.

Badziak, J., Jabłoński, S. & Głowacz, S. (2006). Generation of collimated high-current ion beams by skin-layer laser-plasma interaction at relativistic laser intensities. *Appl. Phys. Lett.* **89**, 061504/1–3.

Badziak, J. (2007). Laser-driven generation of fast particles. *Opto-Electron. Rev.* **15**, 1.

Badziak, J., Jabłoński, S. & Wołowski, J. (2007). Progress and prospect of fast ignition of ICF targets. *Plasma Phys. Contr. Fusion* **49**, B651–B666.

Badziak, J., Jabłoński, S., Parys, P., Rosiński, M., Wołowski, J., Szydłowski, A., Antici, P., Fuchs, J. & Mancic, A. (2008). Ultraintense proton beams from laser-induced skin-layer ponderomotive acceleration. *J. Appl. Phys.* **104** 063310/1–6.

Borghesi, M., Fuchs, J., Bulanov, S.V., Mackinnon, A.J., Patel, P.K. & Roth, M. (2006). Fast ion generation by high-intensity laser irradiation of solid targets and applications. *Fusion Sci. Technol.* **49**, 412–438.

Denevit, J. (1992). Absorption of high-intensity subpicosecond laser on solid density targets. *Phys. Rev. Lett.* **69**, 3052–3055.

Fernandez, J.C., Honrubia, J.J., Albright, B.J., Flippo, K.A., Gautier, D. Cort, Hegelich, B.M., Schmitt, M.J., Temporal, M. & Yin, L. (2009). Progress and prospects of ion-driven fast ignition. *Nucl. Fusion* **49**, 065004/1–8.

Foord, M.E., Patel, P.K., Mackinnon, A.J., Hatchett, S.P., Key, M.H., Lasinski, B., Town, R.P.J., Tabak, M. & Wilks, S.C. (2007). MeV proton generation and efficiency from an intense laser irradiated foil. *High Energy Dens. Phys.* **3**, 365–370.

Fuchs, J., Sentoku, Y., d'Humières, E., Cowan, T.E., Cobble, J., Audebert, P., Kemp, A., Nikroo, A., Antici, P., Brambrink, E., Blazevic, A., Campbell, E.M., Fernández, J.C., Gauthier, J.C., Geissel, M., Hegelich, M., Karsch, S., Pepescu, H., Renard-LeGalloudec, N., Roth, M., Schreiber, J., Stephens, R. & Pépin, H. (2007). Comparative spectra and efficiencies of ions laser-accelerated forward from the front and rear surfaces of thin solid foils. *Phys. Plasmas* **14**, 053105/1–13.

Habara, H., Kodama, R., Sentoku, Y., Izumi, N., Kitagawa, Y., Tanaka, K.A., Mima, K. & Yamanaka, T. (2003). Momentum distribution of accelerated ions in ultra-intense laser-plasma interactions via neutron spectroscopy. *Phys. Plasmas* **10**, 3712–3716.

Hegelich, B.M., Albright, B., Audebert, P., Blazevic, A., Brambrink, E., Cobble, J., Cowan, T., Fuchs, J., Gauthier, J.C., Gautier, C., Geissel, M., Habs, D., Johnson, R., Karsch, S., Kemp, A., Letzring, S., Roth, M., Schramm, U., Schroeiber, J., Witte, K.J. & Fernandez, J.C. (2005). Spectral properties of laser accelerated mid-Z MeV/u ion beams *Phys. Plasmas* **12**, 056314/1–5.

Holkundkar, A.R. & Gupta, N.K. (2008). Effect of initial plasma density on laser induced ion acceleration. *Phys. Plasmas* **15**, 123104/1–10.

Hora, H., Badziak, J., Boody, F., Hopfel, R., Jungwirth, K., Kralikova, B., Krasa, J., Laska, L., Parys, P., Perina, P., Pfejfer, K. & Rohlena, J. (2002). Effects of picosecond and ns laser pulses for giant ion source. *Optics Commun.* **207**, 333–338.

Lee, K., Park, S.H., Cha, Y.-H., Lee, J.Y., Lee, Y.W.,Yea, K.-H. & Jeong, Y.U. (2008). Generation of intense proton beams from plastic targets irradiated by an ultraintense laser pulse. *Phys. Rev. E* **78**, 056403/1–4.

Liseykina, T.V. & Macchi, A. (2007). Features of ion acceleration by circularly polarized laser pulses. *Appl. Phys. Lett.* **91**, 171702/1–3.

Liseykina, T.V., Borghesi, M., Macchi, A. & Tuveri, S. (2008). Radiation pressure acceleration by ultraintense laser pulses. *Plasma Phys. Contr. Fusion* **50**, 124033/1–9.

McKenna, P., Lindau, F., Lundh, O., Carroll, D.C., Clarke, R.J., Ledingham, K.W.D., McCanny, T., Nelly, D., Robinson, A.P.L., Robson, L., Simpson, P.T., Wahistrom, C-G. & Zepf, M. (2007). Low-and medium-mass ion acceleration driven by petawatt laser plasma interactions. *Plasma Phys. Contr. Fusion* **49**, B223–B231.

Pukhov, A. (2001). Three-dimensional simulations of ion acceleration from a foil irradiated by a short-pulse laser. *Phys. Rev. Lett.* **86**, 3562–3565.

Robinson, A., Zepf, M., Kar, S., Evans, R.G. & Bellei, C. (2008). Radiation pressure acceleration of thin foils with circularly polarized laser pulses. *New J. Phys.* **10**, 033034/1–13.

Robson, L., Simpson, P.T., Clarke, R.J., Ledingham, K.W.D., Lindau, F., Lundh, O., McCanny, T., Mora, P., Neely, D.,

Wahlstrom, C.G., Zepf, M. & McKenna, P. (2007). Scaling of proton acceleration driven by petawatt-laser-plasma interactions. *Nature Physics* **3**, 58/1–4.

Sadighi-Bonabi, R., Hora, H., Riazi, Z.,Yazdani, E. & Sadighi, S.K. (2010). Generation of plasma blocks accelerated by nonlinear forces from ultraviolet KrF laser pulses for fast ignition. *Laser Part. Beams* **28**, 101–107.

Roth, M., Blazevic, A., Geissel, M., Schlegel, T., Cowan, T.E., Allen, M., Gauthier, J.C., Audebert, P., Fuchs, J., Meyerter-Vehn, J., Hegelich, M., Karsch, S. & Pukhov, A. (2002). Energetic ions generated by laser pulses: A detailed study on target properties. *Phys. Rev. Spec. Top.* AB **5**, 061301/1–8.

Sentoku, Y., Bychenkov, V.Y., Flippo, K., Maksimchuk, A., Mima, A., Mourou, G., Sheng, Z.M. & Umstadter, D. (2002). High + energy ion generation in interaction of short laser pulse with high-density plasma. *Appl. Phys.* B **74**, 207–215.

Snavely, R.A., Key, M.H., Hatchett, S.P., Cowan, T.E., Roth, M., Phillips, T.W., Stoyer, M.A., Henry, E.A., Sangster, T.C., Singh, M.S., Wilks, S.C., MacKinnon, A., Offenberger, A., Pennington, D.M., Yasuike, K., Langdon, A.B., Lasinski, B.F., Johnson, J., Perry, M.D. & Campbell, E.M. (2000). Intense high-energy proton beams from petawatt-laser irradiation of solids. *Phys. Rev. Lett.* **86**, 1769–1772.

Szydłowski, A., Badziak, J., Fuchs, J., Kubkowska, M., Parys, P., Rosiński, M., Suchańska, R., Wołowski, J., Antici, P. & Mancic, A. (2009). Application of solid-state nuclear track detectors of the CR-39/PM-355 type for measurements of energetic protons emitted from plasma produced by an ultra-intense laser. *Radiat. Meas.* **44**, 881–884.

Temporal, M., Honrubia, J.J. & Atzeni, S. (2002). Numerical study of fast ignition of ablatively imploded deuterium-tritium fusion capsules by ultra-intense proton beams. *Phys. Plasmas* **9**, 3098–3107.

Umstadter, D. (2001). Review of physics and applications of relativistic plasmas driven by ultra-intense lasers. *Phys. Plasmas* **8**, 1774–1785.

Wilks, S.C., Kruer, W.L., Tabak, M. & Langdon, A.B. (1992). Absorption of ultra-intense laser pulses. *Phys. Rev. Lett.* **69**, 1383–1386.

Wilks, S.C., Langdon, A.B., Cowan, T.E., Roth, M., Singh, M., Hatchett, S., Key, M.H., Pennington, D., MacKinnon, A. & Snavely, R.A. (2001). Energetic proton generation in ultra-intense laser-solid interactions. *Phys. Plasmas* **8**, 542–549.

Xu, M.H., Li, Y.T., Yuanet, X.H., Yu, Q.Z., Wang, S.J., Zhao, W., Wen, X.L., Wang, G.C., Jiao, C.Y., He, Y.L., Zhang, S.G., Wang, X.X. Huang, W.Z. Gu, Y.G. & Zhang, J. (2006). Effects of shock waves on spatial distribution of proton beams in ultrashort laser-foil interactions. *Phys. Plasmas* **13**, 104507/1–4.

Yang, X.H., Ma, Y.Y., Shao, F.Q., Xu, H., Yu, M.Y., Gu, Y.Q., Yu, T.P., Yin, Y., Tian, C.L. & Kawata, S. (2010). Collimated proton beam generation from ultraintense laser-irradiated target. *Laser Part. Beams* **28**, 319–325.

Yin, L., Albright, B.J., Hegelich, B.M. & Fernandez, J.C. (2006). GeV laser ion acceleration from ultrathin targets: The laser break-out afterburner. *Laser Part. Beams* **24**, 291–297.

https://doi.org/10.1017/S0263034610000649 Published online by Cambridge University Press